一种 X 射线成像系统模型及其快速标定方法

田　原[1]，　都　东[1]，　侯润石[1]，　高志凌[2]，　申立群[2]
（1. 清华大学 机械工程系，北京　100084；2. 中国华油钢管有限公司，河北 青县　062650）

田　原

摘　要：利用 X 射线进行工件内部缺陷检测是目前应用最广泛的无损检测方法之一，基于图像处理的自动检测技术是其主要发展方向。系统成像模型的建立和标定确定了成像目标与其图像之间的几何对应关系，是利用图像进行自动定位与测量的前提。在忽略一些非线性因素如图像增强器输入屏形状等的情况下，针对用于大直径螺旋钢管焊缝缺陷自动检测的射线成像系统，提出一种简便、可操作性强的方法进行建模并进行标定，结果表明了所采用方法的有效性。

关键词：射线检测；焊缝缺陷；成像模型；标定
中图分类号：TP391.4　　文献标识码：A　　文章编号：0253－360X(2007)07－025－04

0　序　　言

利用 X 射线进行焊缝内部缺陷检测是目前最为可靠且应用最广泛的无损检测方法之一。而基于 X 射线实时成像技术的焊缝缺陷自动检测技术一直是相关领域的研究热点。

由于计算机是基于图像进行缺陷判断和测量，因此必须建立真实场景与其相应图像之间在位置、尺寸、形状等方面的对应关系，也就是对系统的成像过程建立数学模型。这里所说的数学模型指的是系统的几何模型，即物体的三维坐标与其相应的二维数字图像坐标之间的关系。

对于 X 射线成像系统，国内外已有了一些建模和标定方法[1－3]，但大都采用了一些优化或者迭代算法，使得结果不稳定和可操作性变差，作者针对用于大直径螺旋缝钢管焊接缺陷自动检测的射线成像系统，在精度允许范围内，忽略了一些非线性因素如图像增强器输入屏形状、电磁干扰等，提出一种可操作性强的方法进行系统建模和标定，试验结果表明了所采用方法的有效性。

1　成像系统模型的建立

系统结构如图 1 所示。成像系统模型即对系统成像过程的数学描述。借助于成像模型，目标就可以与其图像之间建立位置和形状尺度上的精确映射。为此需要引入几个坐标系统用来描述目标在成像各个环节中的对应关系。

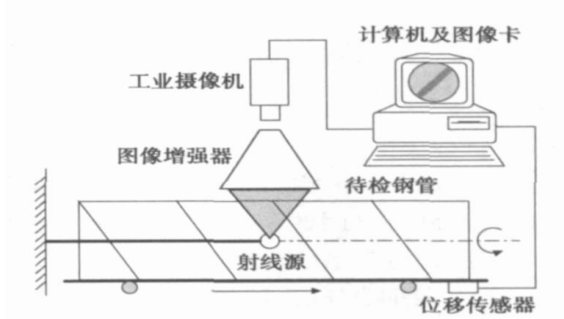

图 1　系统组成
Fig. 1　System configuration

1.1　几个坐标系

如图 2 所示，$\bar{O}\bar{X}\bar{Y}\bar{Z}$ 为世界坐标系，定义其 $\bar{Z}$ 轴与图像增强器中心轴重合，$\bar{Y}$ 轴方向与钢管轴线方向一致，原点与射线源重合。$OXYZ$ 为钢管坐标系，其三个坐标轴方向与世界坐标系的坐标轴方向一致，原点在钢管轴线上。$O'xyz$ 为摄像机坐标系，原点在摄像机光心，z 轴与摄像机轴线一致。

1.2　系统模型

设钢管坐标系原点在世界坐标系中的坐标为 $(\bar{X}_0, \bar{Y}_0, \bar{Z}_0)$，则钢管表面特征点 $m(X_m, Y_m, Z_m)$ 在世界坐标系中的坐标为 $(X_m-\bar{X}_0, Y_m-\bar{Y}_0, Z_m-\bar{Z}_0)$。如图 3 所示，设图像增强器输入屏与射线源之间的距离为 r，则特征点在输入屏上的投影坐标 $(\bar{X}_m, \bar{Y}_m, \bar{Z}_m)$

收稿日期：2006－08－16
基金项目：高等学校博士学科专项科研基金资助项目(20050003041)

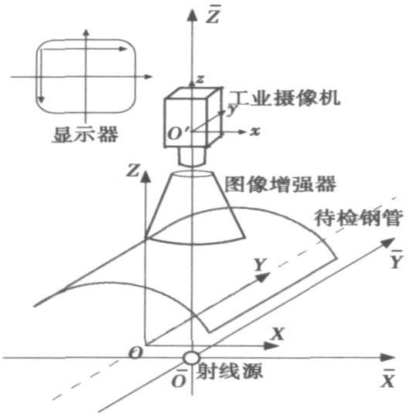

图 2 坐标系

Fig. 2 Sketch of some coordinate systems

可由下式求出

$$\frac{\bar{X}_m}{X_m-\bar{X}_0}=\frac{\bar{Y}_m}{Y_m-\bar{Y}_0}=\frac{\bar{Z}_m}{Z_m-\bar{Z}_0}=\frac{r}{Z_m-\bar{Z}_0},\quad(1)$$

即

$$\begin{cases}\bar{X}_m=\dfrac{X_m-\bar{X}_0}{Z_m-\bar{Z}_0}\cdot r=k\cdot(X_m-\bar{X}_0),\\ \bar{Y}_m=\dfrac{Y_m-\bar{Y}_0}{Z_m-\bar{Z}_0}\cdot r=k\cdot(Y_m-\bar{Y}_0),\end{cases}\quad(2)$$

式中：$k=g(Z_m)=r/Z_m-\bar{Z}_0$，通常大直径钢管的直径都超过 500 mm，因此视场中的钢管可近似为平面，即 k 可近似为常数，或者可以将 (X_m, Y_m) 看作 (X_m, Y_m, Z_m) 在垂直于 Z 轴的平面上的投影。

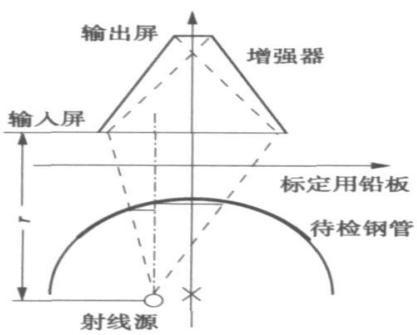

图 3 标定方案

Fig. 3 Sketch of calibration method

以齐次坐标的形式，二者之间的关系可写为

$$\begin{pmatrix}\bar{X}_m\\ \bar{Y}_m\\ 1\end{pmatrix}=\begin{pmatrix}k & 0 & -k\bar{X}_0\\ 0 & k & -k\bar{Y}_0\\ 0 & 0 & 1\end{pmatrix}\cdot\begin{pmatrix}X_m\\ Y_m\\ 1\end{pmatrix}。\quad(3)$$

图像增强器内部变换可看作线性放大，放大系数为 $a\in(0,1)$，则输出屏上的像点 $(\bar{X}'_m, \bar{Y}'_m, \bar{Z}'_m)$ 可表示为

$$\begin{pmatrix}\bar{X}'\\ \bar{X}'\\ 1\end{pmatrix}=-a\cdot\begin{pmatrix}\bar{X}'_m\\ \bar{X}'_m\\ 1\end{pmatrix}。\quad(4)$$

不考虑 Z 轴坐标，仅作为平面投影，则图像增强器输出屏上的点 $(\bar{X}'_m, \bar{Y}'_m, \bar{Z}'_m)$ 与图像平面中对应的像点 (u, v) 之间的关系可用下式表示

$$\begin{pmatrix}u\\ v\\ 1\end{pmatrix}=\begin{pmatrix}a_{11} & a_{12} & a_{13}\\ a_{21} & a_{22} & a_{23}\\ a_{31} & a_{32} & a_{33}\end{pmatrix}\cdot\begin{pmatrix}\bar{X}'_m\\ \bar{Y}'_m\\ 1\end{pmatrix},\quad(5)$$

可表示为

$$\begin{pmatrix}u\\ v\\ 1\end{pmatrix}=\boldsymbol{A}\cdot\begin{pmatrix}\bar{X}'_m\\ \bar{Y}'_m\\ 1\end{pmatrix},\quad(6)$$

式中：$\boldsymbol{A}$ 为摄像机成像转换矩阵，包含摄像机位姿变换以及像素尺度变换因子等参数，则钢管表面特征点 (X_m, Y_m, Z_m) 与其在图像中对应的像点 (u, v) 之间的关系可表示为

$$\begin{pmatrix}u\\ v\\ 1\end{pmatrix}=B\cdot\begin{pmatrix}X_m\\ Y_m\\ 1\end{pmatrix},\quad(7)$$

式中：

$$B=-a\cdot\boldsymbol{A}\begin{pmatrix}k & 0 & -k\bar{X}_0\\ 0 & k & -k\bar{Y}_0\\ 0 & 0 & 1\end{pmatrix}。\quad(8)$$

式(7)即为系统的成像模型，其中忽略了图像增强器因电磁干扰引起的成像畸变以及摄像机自身带来的成像畸变。理论分析表明，摄像机成像畸变的影响随着到图像中心距离的增加而增大[4]。

2 系统标定

标定是确定数学模型中各未知参数从而确定实际场景与其图像之间对应关系的过程，这些参数有的是设备自身或者安装过程给出但精度不足或者安装时有所改变的，有的属于设备没有给出但可以实测的，有的是无法直接测量或测量有困难的，都需要通过系统标定来确定。

成像系统标定本身在计算机视觉领域中是一个

重要的研究方向，其方法主要包括两类，一类是传统的基于已知场景的标定方法，一类是自标定方法[5]。出于计算和操作的复杂性和标定可靠性的考虑，选用传统标定方法，即利用一已知若干(小于 4)个三维特征点相对位置的标定物体，测出这些特征点所对应的像点位置，借助于所建立的成像系统数学模型，利用最小二乘法即可获得投影矩阵，从而确定真实物体中三维点与其图像中三维点之间的投影关系，由此实现缺陷形状尺寸和位置的测量。如图 4 所示为试验中所用的标定物体，图 4a 为其设计图，即一块厚度约 4 mm、均布若干孔(孔间距已知)的铅板，图 4b为其图像(已经过二值化并通过图像处理的方法标出其几何中心)。

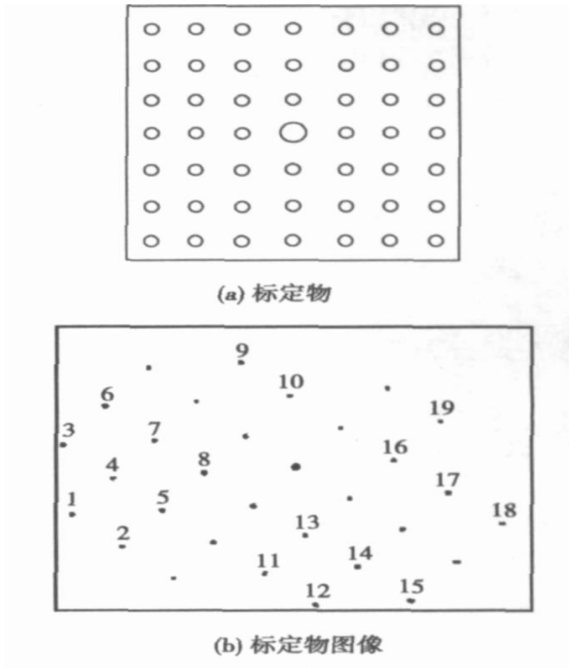

图 4　标定物及其图像

Fig. 4　Calibration object and its image

3　试验结果

为了验证系统模型的准确性和标定效果，试验分为投影和逆投影两部分。表 1 是投影试验结果，表2 是逆投影试验结果。其中所有带有标号(1 ~ 19)的点为验证点，其它点为控制点，如图 4b 所示。

表 1　投影结果

Table 1　Data about projection

序号	理论坐标 (x_t, y_t)(像素)	实测坐标 (x_r, y_r)(像素)	偏差 d(像素)	序号	理论坐标 (x_t, y_t)(像素)	实测坐标 (x_r, y_r)(像素)	偏差 d(像素)
1	(43, 676)	(28, 682)	16	11	(561, 890)	(560, 892)	2
2	(176, 792)	(167, 798)	11	12	(696, 1 002)	(698, 1 008)	6
3	(18, 426)	(7, 429)	11	13	(669, 751)	(676, 754)	8
4	(151, 545)	(144, 544)	7	14	(809, 866)	(814, 869)	6
5	(286, 661)	(283, 660)	3	15	(955, 987)	(952, 985)	4
6	(131, 287)	(123, 290)	8	16	(907, 482)	(908, 477)	5
7	(265, 409)	(261, 406)	5	17	(1 053, 595)	(1 047, 593)	6
8	(397, 526)	(398, 522)	4	18	(1 202, 706)	(1 185, 708)	17
9	(495, 129)	(493, 129)	2	19	(1 033, 340)	(1 025, 339)	8
10	(628, 250)	(631, 245)	6				

表 2　逆投影结果

Table 2　Data about converse projection

序号	理论坐标 (x_t, y_t)/mm	实测坐标 (x_r, y_r)/mm	偏差 d/mm	序号	理论坐标 (x_t, y_t)/mm	实测坐标 (x_r, y_r)/mm	偏差 d/mm
1	(－49.848, －75)	(－48.855, －72.938)	2.288 6	11	(24.968, －50)	(24.836, －49.657)	0.367 5
2	(－24.968, －75)	(－24.522, －73.436)	1.626 3	12	(49.848, －50)	(49.027, －49.553)	0.934 8
3	(－74.553, －50)	(－73.660, －48.639)	1.627 8	13	(24.968, －25)	(23.922, －25.326)	1.095 6
4	(－49.848, －50)	(－49.060, －49.456)	0.957 5	14	(49.848, －25)	(48.907, －25.097)	0.946 0
5	(－24.968, －50)	(－24.515, －49.777)	0.504 9	15	(74.553, －25)	(75.057, －24.972)	0.504 8
6	(－74.553, －25)	(－74.046, －23.864)	1.244 0	16	(24.968, 25)	(25.216, 24.334)	0.710 7
7	(－49.848, －25)	(－49.075, －24.910)	0.778 2	17	(49.848, 25)	(50.657, 25.308)	0.865 6
8	(－24.968, －25)	(－24.758, －25.604)	0.639 5	18	(74.553, 25)	(76.237, 26.760)	2.435 9
9	(－49.848, 25)	(－49.601, 25.206)	0.321 6	19	(24.968, 50)	(25.937, 50.581)	1.129 8
10	(－24.968, 25)	(－24.825, 24.177)	0.835 3				

从表 1, 表 2 中数据可知, 处于图像中心区域的验证点 5, 7, 8, 10, 11, 13, 14, 16 的投影平均偏差为 4.875 像素, 逆投影平均位置偏差为 0.730 mm; 而远离中心的其它验证点的投影平均偏差为 8.727 像素, 逆投影平均位置偏差为 1.267 mm。这一结果表明, 受摄像机成像畸变、图像增强器电磁干扰引起的成像畸变的影响随着验证点于图像中心距离的增加而增大。

投影与逆投影结果可更直观地用图 5, 图 6 表示。

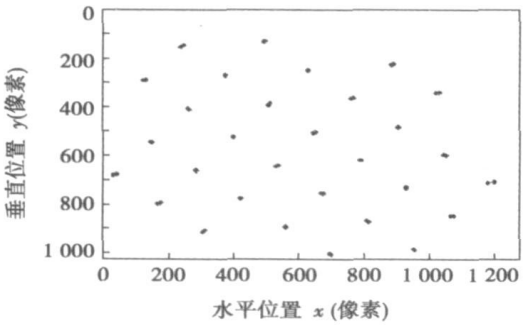

图 5 投影结果

Fig. 5 Projection result

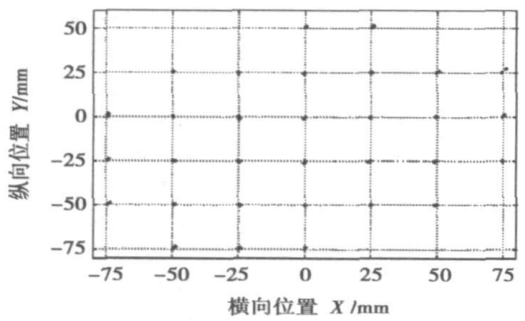

图 6 逆投影结果

Fig. 6 Converse projection result

4 结 论

成像系统建模是利用图像进行自动定位与测量的前提; 系统标定则是利用一定途径求解系统模型中各未知参数的过程。实际应用中, 在满足测量精度的前提下, 标定过程的可操作性和结果的稳定可靠往往更重要, 针对用于大直径螺旋钢管焊缝缺陷自动检测的射线成像系统, 提出一种可操作性强的方法进行建模和标定, 试验结果表明了所采用方法的有效性, 同时证明图像中心区域的成像畸变小于边缘区域的成像畸变, 这一结论对于图像处理中 ROI(region of interesting)位置的选择有指导意义。

参考文献:

[1] Domingo Mery, Dieter Filbert. Automated flaw detection in aluminum castings based on the tracking of potential defects in a radioscopic image sequence [J]. IEEE Transactions on Robotics and Automation, 2002, 18(6): 890−900.

[2] 任大海, 尤 政, 郑继贵, 等. 射线实时成像检测系统透视变换模型[J]. 光学技术, 2000, 26(2): 134−138.

[3] Domingo Mery. Explicit geometric model of a radioscopic imaging system [J]. NDT&E International, 2003, 36: 587−599.

[4] Milan Sonka, Vaclav Hlavac, Roger Boyle. 图像处理、分析和机器视觉[M]. 艾海舟, 武 勃, 译. 北京: 人民邮电出版社, 2003.

[5] 邱茂林, 马颂德, 李 毅. 计算机视觉中摄像机定标综述[J]. 自动化学报, 2000, 26(1): 43−55.

作者简介: 田 原, 男, 1976 年出生, 博士研究生。主要研究方向为图像处理、射线探伤等。发表论文 7 篇。

Email: tianyo2@mails.tsinghua.edu.cn

Nanjing University of Technology, Nanjing 210009, China; 2. School of Mechanical and Power Engineering, East China University of Science and Technology, Shanghai 200237, China). p17—20

Abstract: The residual stress generated in brazed process and its creep relaxation behavior for stainless steel plate-fin structure at high temperature were analyzed by finite element code-ABAQUS. The results show that larger residual stress was generated in brazed joint due to the mismatch mechanical properties between brazing filler metal and base metal and the constraint of clamping fixture. At high temperature region, the residual stress was greatly decreased due to the creep relaxation behavior. The creep stress and strain are concentrated in the fillet zone, where the crack may initiate and propagate along the brazing seam.

Key words: stainless steel plate-fin structure; brazing residual stress; creep relaxation; finite element analysis

Microstructure and wear resistance of laser cladding Co+Ni/WC alloy composite coating YAN Yonggen[1], SI Songhua[2], ZHANG Hui[2], HE Yizhu[2] (1. Baoshan Iron & Steel Co., Ltd, Shanghai 201900, China; 2. School of Material Science and Engineering, Anhui University of Technology, Maanshan 243002, Anhui, China). p21—24

Abstract: Laser cladding Co-based composite coating (Co+Ni/WC) have been obtained on low carbon steel substrate. Microstructure and wear resistance of the composite coatings were investigated compared with the Co-based coating (Co60). It is indicated that the Co60 coating was composed of primary dendrite of γ—Co and the eutectics of γ—Co+$Cr_{23}C_6$ among the interdendritics, and Co+Ni/WC composite coatings were composed of γ—Co dendrite and the small eutectics, which consists of γ—Co, Cr_7C_3, Co_3W_3C and unmelted WC particles. With more WC particles, there was further influence to Co60 coating that the directional solidification of dendrite was changed and the dendrite was finer. Owing to the Ni alloy wrapper, the WC particles had been protected from melt for the diffusion reaction on interface between the WC particles and the Co based alloy. Compared with Co60 coating, the hardness and wear resistance of the Co+Ni/WC composite coatings had been improved and the wear resistance of the Co+20%WC composite coating was twice of that of the Co60 coating.

Key words: laser cladding; Co-based alloy; microstructure; wear resistance

An imaging model for X-ray system and its calibration method TIAN Yuan[1], DU Dong[1], HOU Runshi[1], GAO Zhiling[2], SHEN Liqun[2] (1. Department of Mechanical Engineering, Tsinghua University, Beijing 100084, China; 2. Petroleum Steel Pipe Co., Ltd, Qingxian 062650, Hebei, China). p25—28

Abstract: It's one of the most extensive methods to inspect workpiece with X-ray and automatic inspection based on image processing is an important field. The imaging model and calibration establish a geometrical relationship between workpiece and its image, which is the precondition for automatic orientation and measurement with images. Ignored some factors such as the shape of the image intensifier's input screen, the paper develops a model and calibration method for the imaging system used in automatic nondestructive testing system, which is used in weld defect inspection. The results show that the method is effective.

Key words: inspection with X-ray; weld defect; imaging model; calibration

Corrosion of carbon steel joint used modified J422 electrode in ammonium sulfite LEI Ali, ZHANG Shengchao, ZHANG Min (School of Materials Science and Engineering, Xi'an University of Technology, Xi'an 710048, China). p29—32

Abstract: Since the welded joint of carbon steel is corroded seriously in the ammonium sulfite, corrosion behavior of welded joint welded by arc welding with J422 electrode containing different contents of Ni has been studied by means of three electrode galvanochemistry test and metallurgical structure analyses. The results show that the addition of Ni causes the grain refinement of the weld and the decrease of acicular ferrite. In addition, the polarizability of the weld increases and the corrosion current decreases in the ammonium sulfite. The welded joint containing 1.2 wt% Ni has the lowest corrosion rate.

Key words: ammonium sulfite; weld decay; alloying; galvano-chemistry

Displacement signal time-frequency domain analysis and quality judgment of aluminum alloy resistance spot welding PAN Cunhai[1], DU Sumei[1], SONG Yonglun[2] (1. School of Mechanical Engineering, Tianjin University of Science and Technology, Tianjin 300222, China; 2. School of Electromechanical Engineering, Beijing University of Technology, Beijing 100085, China). p33—36

Abstract: Resistance spot welding quality real-time monitoring of aluminum alloy was realized by distributed multiple-sensor synchronous collection system. Displacement signal time-frequency domain analysis shows that Butterworth band-pass filter range of the expulsion welding spot electrode displacement signal can reach about 0.5 mm between 40—80 Hz. The electrode displacement signal range of the undersize welding spots is lower about 1.0 mm than other two kinds of welding spots, so that using the explicit characteristic information can implement at resistance spot welding quality judgment by man and further can finish quality judgment by machine using the high signal-to-noise displacement signal and the brevity characteristic extracting method. At the same time, statistic analysis of 197 samples indicates that the percentage of accuracy can reach 97.6% at the acceptable welding spots zone.

Key words: resistance spot welding; aluminum alloy; displacement signal; time-frequency domain analysis; quality judgment

Numerical simulation on flow and heat transfer in weld pool of laser-plasma hybrid welding LI Zhining, DU Dong, CHANG Baohua, WANG Li (Key Laboratory for Advanced Materials Processing Technology, Ministry of Education, Tsinghua University, Beijing 100084, China). p37—40

Abstract: A unified model is establtshed for the liquid zone,